JACS
JOURNAL OF THE AMERICAN CHEMICAL SOCIETY
Article
pubs.acs.org/JACS

Mechanism of Singlet Fission in Thin Films of 1,3-Diphenylisobenzofuran

Joel N. Schrauben,[†] Joseph L. Ryerson,[†,‡] Josef Michl,[‡,§] and Justin C. Johnson*[,†]

[†]National Renewable Energy Laboratory, Golden, Colorado 80401, United States
[‡]Department of Chemistry and Biochemistry, University of Colorado, Boulder, Colorado 80301, United States
[§]Institute of Organic Chemistry and Biochemistry, Academy of Sciences of the Czech Republic, Flemingovo náměstí 2, 16610 Prague 6, Czech Republic

Supporting Information

ABSTRACT: In order to elucidate the mechanism of singlet fission in thin films of 1,3-diphenylisobenzofuran (**1**) we have performed ultrafast transient absorption spectroscopy as a function of sample temperature and excitation fluence on polycrystalline thin films composed of two polymorphs. Our earlier investigations revealed that films enriched in a particular polymorph of **1** displayed near 200% efficiency for triplet formation at 77 K, while films composed primarily of a second polymorph had a very low triplet quantum yield. Present data confirm the triplet yield disparities in the two polymorphs and demonstrate the distinct fates of the initially prepared singlets in films of different structure. Singlet fission is inhibited in the more stable polymorph due to rapid excimer formation and trapping. The less stable polymorph undergoes highly efficient singlet fission with a dominant time constant of 10−30 ps and without strong thermal activation. Transient absorption measurements with varying excitation fluence indicate that singlet−singlet annihilation is a primary competitor of singlet fission at higher fluence and that fission from higher-lying states can also contribute to the triplet formation process. Measurements employing different excitation energies and sample temperatures reveal the role that trapping processes play in attenuating the triplet quantum yield to produce the complex temperature dependence of the singlet fission yield. The rate constants for singlet fission itself are essentially temperature independent.

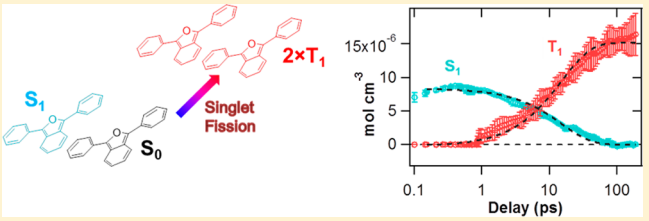

I. INTRODUCTION

Singlet exciton fission (SF) is a photophysical process, observed primarily in single molecular crystals and polycrystalline thin films, wherein a chromophore in an excited singlet state (S_1) interacts with a nearby chromophore in its ground state (S_0) to form two triplet states (T_1) on the two chromophores.[1] The study of SF has been revitalized in recent years as the potential of this process to augment photocurrent production at energies greater than 2 eV in solar photoconversion schemes has become widely recognized.[2]

Our groups have been studying SF in thin films and dimers of 1,3-diphenylisobenzofuran (**1**) for several years.[3−7] **1** was identified through first-principle calculations to have the correct energy alignment of S_1 and T_1 states to undergo SF, namely, that $E(S_1)$ is above or near twice the energy of T_1.[6] The S_1 and T_1 energies of isolated **1** were later reported as $E(S_1)$ = 22 000 cm^{-1} and $E(T_1)$ = 11 400 cm^{-1}, making SF from S_1 slightly endothermic (~800 cm^{-1}).[7] The initial report on thin films of **1**[4] revealed two polymorphs, now called α and β, that differ in their photophysical properties. Films of α-**1** undergo efficient SF, producing two triplets for every absorbed photon at 80 K and ~1.3 triplets per photon at room temperature. Films of β-**1** have triplet quantum yields (Φ_T) that are about 0.10.[5] SF in α-**1** occurs with biexponential kinetics, exhibiting time constants of ~2 and ~25 ps when the rise of T_1-T_n absorptions is monitored.

Outstanding questions regarding the film composition and structure are addressed in a separate publication.[8] This report deals primarily with understanding the triplet formation mechanism in α-**1**. Steady-state and time-resolved spectroscopy are implemented to investigate the origin of the complex temperature dependence of Φ_T and the two distinct time constants for triplet formation. While both polymorphs exhibit photophysical processes that compete with SF, measurements on β-**1** films reveal rapid photophysical processes that nearly completely quench SF.

A fairly large number of molecular crystals or thin films have been recently shown to exhibit SF,[9−18] and a simplistic view of SF competing only with prompt fluorescence from a locally excited singlet state is probably not accurate in many cases. In actuality, when intermolecular geometries appropriate for SF are engendered, other species besides a triplet pair may also be formed that complicate the kinetic scheme. **1** does not present a simple system in which SF is competing solely with fluorescence; in addition to radiative decay, annihilation processes (especially when excited at higher excitation fluence),

Received: February 7, 2014
Published: April 15, 2014

   dx.doi.org/10.1021/ja501337b | J. Am. Chem. Soc. 2014, 136, 7363−7373

activated SF pathways, and the possibility of heterogeneity due to the presence of polymorphs must be considered. The temperature dependence of the triplet yield can be particularly complicated, as the temperature dependence of the unit cell volume,[8] the strong dependence of SF rate constants on interchromophore spacing and slipping modulated by lattice deformation,[19−23] and the possible presence of activation barriers for competing processes like trapping are combined to produce the measured temperature dependence.[1,5,24,25] Indeed, tetracene was considered to be the prototypical example following standard theory,[26] but it is now known to be more complex in the sense that a simple interplay between prompt fluorescence and SF is not valid at all temperatures.[27−29] A global view of all photophysical processes in addition to SF can be challenging in some systems but is the goal of the present work.

II. EXPERIMENTAL SECTION

General. Fused silica, glass, sapphire, quartz, and indium-doped tin oxide conducting glass (ITO) substrates (Thin Film Devices, Inc.) were rinsed with acetone and isopropyl alcohol followed by an O_2 plasma cleaning step. Powdered **1** (97%) used in these experiments was obtained from Aldrich. Films were prepared by either thermal evaporation or solution drop-casting, as described in more detail in ref 8.

The film composition is presented as the fraction of α crystallites (χ_α), determined for each film by using the empirical relationship between the vibronic intensities in the absorption spectra and the XRD diffraction peaks (Figure 5 in the companion paper[8]). The same relationship is used throughout the main text and Supporting Information (SI) to indicate the character of each film. For films with a high fraction of β crystallites, the available data were extrapolated to estimate χ_α. The relationship is modeled with $\chi_\alpha = 2.003(A_2{:}A_1) - 1.33$, where $A_2{:}A_1$ is the ratio of the absorbances of the first (A_1) and second (A_2) vibronic features. Although the XRD data indicate that χ_α for β-**1** films can be nearly zero, these films are reported as $\chi_\alpha < 0.1$ due to the error introduced in the above method from the absorbance measurements as a result of the highly scattering nature of β-**1** films.

Steady-State Spectroscopic Measurements. Optical extinction spectra were collected using a Varian Cary 500 Scan UV−vis−NIR spectrophotometer with a scan speed of 600 nm/min and a scan range of 200−800 nm. The baseline was collected in dual-beam mode with blank substrates in both the sample and reference beam paths. Sample data were referenced against a blank substrate in the reference beam path. No accounting for scattering or reflection was made with this instrument. Corrected integrating sphere absorption measurements are a more accurate representation of the pure absorbance of these films. A Shimadzu UV-3600 UV−vis−NIR spectrophotometer with an integrating sphere was used to measure transmittance (T) as well as reflectance (R) (scattering). The optical density (OD) of these films can be calculated from $OD = -\log(R + T)$.

Steady-state fluorescence measurements were performed with a Horiba Jobin Yvon model FL-1039/40 Fluorolog, a Horiba Jobin Yvon iHR320 spectrograph, and a Horiba Jobin Yvon SPEX Instruments S.A. Group Spectrum One G35 CCD camera.

Transient Absorption. Due to the sensitivity of films of **1** to ambient conditions as well as reduced pressure, all films intended for transient absorption experiments were sealed under inert conditions using a Surlyn frame and a top glass slide by heating the entire assembly on a hot plate at 90 °C for 5−10 s. Ultrafast pump−probe experiments were carried out as described previously.[7] Briefly, the 12 900 cm^{-1}, 600 μJ output of a Clark CPA-2001 laser was split 90:10. The stronger portion was frequency-doubled to produce the excitation pulse at 25 800 cm^{-1}, with the pulse energy reduced to $\leq$1 μJ/pulse for all experiments. The excitation beam was modulated at 500 Hz and defocused to a spot size of approximately 0.5 mm to prevent photodamage to the sample and avoid triplet fusion dynamics that can arise at higher fluences. The weaker portion of the beam was focused into a continuously translated CaF_2 crystal to produce a white light continuum (12 500−26 300 cm^{-1}), which was split to use as both a probe and background signal at the sample. These two supercontinuum beams were imaged onto matched Si photodiode arrays to collect full spectra. The data collected by the 1024 pixels of these arrays were binned such that a final spectrum of 102 points was produced. The temporal laser pulse width is ∼150 fs fwhm, and dynamics extending out to ∼400 fs are considered convolved with the instrument response. Data collected with pump−probe delays from −1 to 20 ps were corrected for the chirp of the probe pulse. This procedure produces jagged artifacts in the very early time transient (0−2 ps) spectra that were corrected by a 2D box smoothing method.

Fluence-dependent ultrafast transient absorption measurements on α-**1** films were carried out at 30, 80, 180, and 295 K at 25 800 cm^{-1} excitation using the Clark system. Excitation energies were measured in full and through a 150 μm pinhole to calculate the excitation spot size. Data were analyzed by first fitting the spectra at each pump−probe delay with a model that included extinction spectra of S_0-S_1, S_1-S_n (with stimulated emission features), and T_1-T_n spectra to extract concentration profiles for these states. The fluence-dependent concentration profiles were subsequently fitted in a global fitting procedure with kinetic models that included singlet fission, vibrational cooling, and singlet−singlet annihilation processes (see below and the SI for details).

Angle-dependent ultrafast transient absorption measurements, important to correctly determine Φ_T (see below for a brief description of Φ_T measurements and the SI for further details), were carried out at 25 800 cm^{-1} excitation using the Clark system with films evaporated onto 0.5 mm thick sapphire substrates without a top window, necessary so that probe beam deviation upon angle tuning was minimal. While all measurements were carried out at room temperature, the films were mounted in a cryostat that was briefly pumped down to 10^{-2} Torr and then backfilled with N_2. The films were stable under these inert conditions for the 4−6 h required to complete the experiment. Angles between the probe beam direction and the substrate normal of 0°−45° were achieved by rotating the cryostat head.

Ultrafast transient absorption measurements at low fluence were carried out at 25 600, 23 800, and 22 200 cm^{-1} excitation using a different instrument. The excitation pulses were produced by a Coherent Libra regeneratively amplified Ti:sapphire laser with ∼4 W, 1 kHz, ∼100 fs output at 800 nm; about 30% of this is directed into a TOPAS-C optical parametric amplifier that is capable of producing wavelengths from 300 to 1600 nm as the excitation source. The excitation beam is attenuated and introduced into an Ultrafast Systems Helios spectrometer, and ∼100 μJ of the 800 nm Libra output is also directed into the Helios, passing along a multipass delay stage that can afford ∼5.8 ns of pump−probe delay, and then focused onto a continuously moving CaF_2 crystal to produce a broadband visible spectrum (300−850 nm), used as the probe beam. The probe is passed through a neutral density filter, where a fraction is picked off to be used as a reference to account for fluctuations in the probe intensity. The pump and probe beams are overlapped at the sample with the pump beam having a spot size of ∼250 μm diameter. The excitation is modulated at 500 Hz through an optical chopper to record both pump on and pump off spectra. Photodiode arrays are used for detection of both the probe and reference, and the transient signal is calculated in the Helios software. Typical acquisitions scan 200 ps using 100 points with exponential time spacing, using several forward and reverse scans to average while monitoring for sample degradation. Background and chirp corrections were carried out using the Surface Explorer software (Ultrafast Systems), and other data manipulations and plotting are carried out using Igor Pro 6.34A.

Briefly, Φ_T is calculated according to eq S2 in the SI. This equation includes $\varepsilon_{S1}/\varepsilon_{T1}$, the ratio of the extinction coefficients of S_1-S_n and T_1-T_n absorptions,[7] and r_y^{S1}/r_y^{T1}, a ratio that accounts for the orientation of the transition dipoles of the S_1-S_n and T_1-T_n absorptions in the crystalline films. r_y^{S1}/r_y^{T1} is determined through polarization- and angle-dependent ultrafast transient absorption

dx.doi.org/10.1021/ja501337b | J. Am. Chem. Soc. 2014, 136, 7363−7373

experiments (see the SI). The triplet yields for β-**1** films reported here should be considered upper limits, as the residual S_1-S_n absorptions are likely contributing to the amplitude at the position of the T_1-T_n absorption. To ensure that these angle-dependent measurements were correctly carried out, similar measurements were made on pentacene thin films, revealing an identical angle and polarization dependence to what has been reported in the literature.[14]

Nanosecond transient absorption (flash photolysis) data were collected with a Nd:YAG laser pumped optical parametric oscillator (OPO, Continuum Surelite) and an Edinburgh Instruments model LP920 spectrometer, as described previously.[7] Excitation energies were 0.5−1 mJ/pulse when exciting films at 28 200 cm^{-1} (355 nm) and 0.4−1.5 mJ/pulse for excitations spanning 19 600−24 400 cm^{-1}. Triplet action spectra were constructed by varying the excitation energies from 19 600 to 24 400 cm^{-1} (510−410 nm) in steps of about 5 nm. The triplet absorption feature near 21 000 cm^{-1} was monitored, and the triplet amplitude was extracted from the fit of the data with a monoexponential function. Transient absorption amplitudes were normalized by the excitation power for each excitation wavelength. Error bars on these measurements reflect the error in the power measurement as well as the variation in amplitude across a series of three measurements.

Variable temperature spectroscopic measurements on films were performed using either a liquid nitrogen or a closed-loop He optical cryostat (18−300 K).

III. RESULTS

Film Composition and Steady-State Properties. Figure 1 shows the absorbance and fluorescence spectra of two films of

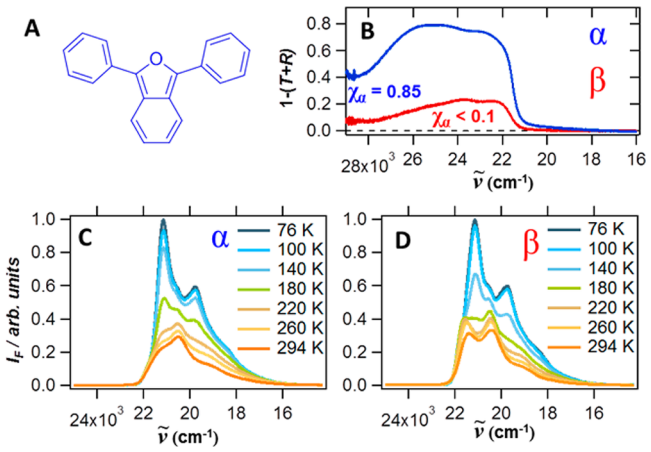

Figure 1. (A) Structure of 1,3-diphenylisobenzofuran (**1**). (B) Absorptance ($1 - (T + R)$) spectra for films composed of mostly α-**1** (blue) and mostly β-**1** (red), collected in an integrating sphere and corrected for the reflectance of the film. Temperature-dependent fluorescence spectra of a mostly α-**1** film (C) and a mostly β-**1** film (D) (fluorescence intensity, I_F, normalized by the observed peak intensity at 76 K).

1, one composed mostly of α-**1** and the other primarily of β-**1**. All thin films of **1** likely contain both α and β polymorphs, with β forming preferentially at the substrate surface and under certain deposition conditions.[8] The films are therefore referred to as composed "mostly" of either α-**1** or β-**1**, and the spectra in Figure 1 contain contributions from both polymorphs. Films of mostly α-**1** employed in this report contain about 15% β-**1** (χ_α = 0.85), while films of β-**1** can be made with nearly no α-**1**, χ_α < 0.1. The absorption spectra of Figure 1B are quite broad, similar to **1** in solution, and α-**1** and β-**1** films clearly have different absorption profiles. The absorption spectra of β-**1** films can be modeled with a single Franck−Condon progression, while the spectra of α-**1** films contain the β-**1** spectrum as well as a series of peaks derived from an H-aggregate model.[8,30] The extinction coefficient for α-**1** films is estimated as 27 600 M^{-1} cm^{-1} at 24 000 cm^{-1}, on the basis of film thicknesses as determined by AFM measurements.[31] A similar determination of the extinction coefficient of β-**1** films is problematic due to the large voids that form between crystallites when these films are prepared. The fluorescence quantum yield, Φ_F, increases as the β-**1** content in a film is increased, from 0.16 for films containing mostly α-**1** up to 0.59 for films of β-**1**. The low temperature fluorescence spectra for a mostly α-**1** film are very similar to those observed in β-**1** films. At room temperature, the films show emission spectra that contain a weak feature that is broad and featureless, centered near 18 000 cm^{-1} (Figure S1, SI). This feature is more pronounced at higher excitation energies and in β-**1** enriched films.

Time-Resolved Fluorescence and Absorption. In the companion study, time-resolved fluorescence decays are presented for both α-**1** and β-**1** films.[8] β-**1** films decay biexponentially, with lifetimes of 1.3 and 3.3 ns. α-**1** films contain two decay components very similar to those observed in the β-**1** films (1.3 and 5 ns) as well as a much faster decay component (an instrument limited ∼380 ps) and a much weaker ∼17 ns component. The ∼17 ns component is much larger than the radiative lifetime of S_1 in isolated **1**, about 6 ns.[7]

Figure 2 displays ultrafast transient absorption spectra after excitation at 25 800 cm^{-1} at 298 K for a series of films deposited on ITO by thermal evaporation and then annealed, spanning from highly α-**1** to highly β-**1** (the entire series is presented in Figure S3 of the SI). Assignments of features in these spectra have been made previously.[4,7] At small pump−probe delays, the α-**1** film (Figure 2A) has negative features arising from the loss of S_0-S_1 absorption (22 000 cm^{-1}) and from stimulated emission from the S_1 state (19 000−20 000 cm^{-1}). Positive features at early delay times arise from excited state S_1-S_n absorptions (21 000 and 15 000−18 000 cm^{-1}); these features have been observed in solutions of **1**.[7] The lower energy S_1-S_n absorption decays concomitantly with the rise of the T_1-T_n absorption, which appears most strongly at 21 500 cm^{-1} and overlaps to some degree both S_0-S_1 and S_1-S_4 and S_1-S_5 features. As the film is annealed, the ratio of β-**1** to α-**1** crystallites increases, and the amplitude of the T_1-T_n absorption decreases, but fast dynamics are observed when monitoring near the T_1-T_n absorption (Figure S3, SI). Moreover, the stimulated emission feature becomes broader and more intense, suggesting emissive contributions from states other than locally excited S_1. For films that are mostly β-**1**, the broad stimulated emission feature overlaps strongly with the S_1-S_n absorptions in the range of 15 000−18 000 cm^{-1}. Films prepared by drop-casting from solution exhibit essentially the same features and triplet yields as vapor-deposited α-**1** and β-**1** films (Figure S2, SI).

The S_1-S_n and T_1-T_n spectra can be extracted in an approximate fashion by adding to the observed transient spectra a scaled amount of the known S_0-S_1 absorption spectrum. The initial concentration of molecules with excitations in the S_1 state, $[S_1]$, is determined at a pump−probe delay of 400 fs, which lies just after the overlap of the pump and probe pulses. The maximum concentration of molecules in the T_1 state, $[T_1]$, is determined at 165 ps. The spectra collected at 400 fs and 165 ps time delay on a film of mostly α-**1** crystallites are shown in Figure 2C,D. Using the molar extinction coefficients measured

dx.doi.org/10.1021/ja501337b | J. Am. Chem. Soc. 2014, 136, 7363−7373

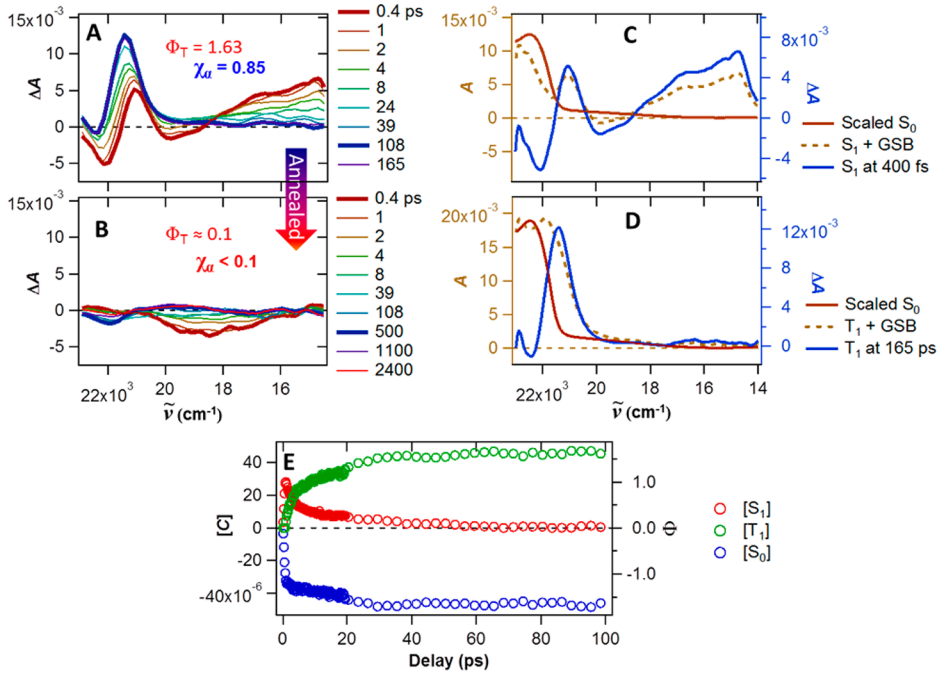

Figure 2. (A) Measured absorbance change ΔA vs time of a mostly α-**1** film at 295 K. (B) Spectra after annealing to create a film of mostly β-**1**. (C) S_1-S_n and (D) T_1-T_n spectra for the α-**1** type film in panel A. *A* is the absorbance of each species determined from the extracted spectrum and GSB is ground state bleach. (E) Extracted state concentrations at each delay time. Terms in brackets indicate their concentration (in units of mol cm^{-3}) and Φ is the yield of population in S_0, S_1, and T_1 states.

for solutions of **1** [$\varepsilon(S_1)$ = 23 400 M^{-1} cm^{-1} at 14 500 cm^{-1}; $\varepsilon(T_1)$ = 32 100 M^{-1} cm^{-1} at 21 800 cm^{-1}; $\varepsilon(S_0)$ = 25 000 M^{-1} cm^{-1}] and the orientation factors in Table S1 (SI), we calculate $[S_1]_{400\ fs}$ = 2.8 × 10^{-5} mol cm^{-3} and $[T_1]_{165\ ps}$ = 4.7 ± 0.2 × 10^{-5} mol cm^{-3}, indicating a 165 ± 10% Φ_T.[32,33] The concentration of molecules with a depleted ground state is assumed to be equal to $[S_1]$ at 400 fs. Using the known S_0-S_1 absorption spectrum and the extracted S_1-S_n and T_1-T_n spectra, the concentrations of S_0, S_1, and T_1 can be extracted at each delay time of the transient absorption experiment (see SI for further details), shown in Figure 2E. In this treatment, the resulting S_1-S_n spectrum also contains the stimulated emission feature. The extracted concentrations as a function of pump−probe delay time are also represented as normalized to the initial $[S_1]$ (Figure 2E, right axis). In addition to the normalized $[T_1]$ reaching values much larger than one at delay times >20 ps, further bleaching of $[S_0]$ concomitant with the rise in $[T_1]$ matches our previous report and offers conclusive evidence for SF.[4]

As the films become further enriched in β-**1** crystallites, the transient absorption measurements become increasingly difficult due to increased light scattering. The top panel of Figure 3 shows a typical series of transient spectra for a β-**1** film, and the lower panels compare the short and long delay time spectra to the extracted S_1-S_n and T_1-T_n absorptions for the α-**1** film from Figure 2. The spectra at delay times greater than 100 ps are somewhat similar to those observed for α-**1** films at longer delays but appear to contain more residual S_1-S_5 absorption. At 400 fs, the transient spectrum is dominated by a broad stimulated emission feature that overlaps strongly with the S_0-S_1 bleach and the S_1-S_n absorptions. The broad stimulated emission is spectrally similar to steady-state fluorescence shown in Figure S1 (SI). Fluorescence excitation spectra were acquired for both mixed composition α/β and highly β films in order to distinguish features characteristic of

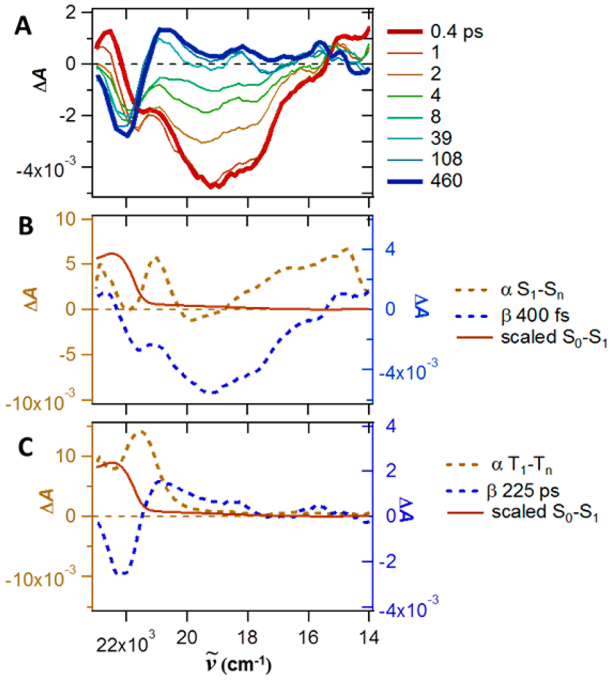

Figure 3. (A) Transient absorption spectra of a mostly β-**1** film ($\chi_\alpha \approx$ 0.25) at 295 K with 25 800 cm^{-1} excitation at delay times indicated. Comparison of the S_0-S_1 absorption and the extracted S_1-S_n and T_1-T_n features from Figure 2 with the (B) short and (C) long delay time features of a β-**1** enriched film.

each crystallite type (Figure S1, SI). When the fluorescence spectra are normalized at 20 355 cm^{-1}, both mixed and highly β-**1** enriched films show slightly larger amplitude at longer wavelengths (largest noticeable amplitude change at 18 940 cm^{-1}) when excited above ~25 000 cm^{-1}. This additional

dx.doi.org/10.1021/ja501337b | J. Am. Chem. Soc. 2014, 136, 7363−7373

fluorescent component is quite broad, which suggests an origin from trapped exciton or excimer species. The broad, red-shifted fluorescence is more pronounced for the film composed mostly of β-**1**. At room temperature the fluorescence spectra of β-**1** can be well described by a Franck−Condon progression with a Huang−Rhys factor of 0.90 and a vibronic spacing of 850 cm^{-1} summed with a broad Gaussian component centered around 18 000 cm^{-1} with a width of ~4000 cm^{-1}.[8] These results are characteristic of fluorescence arising from both the S_1 state and from an excimer/trap state.

The triplet formation onset for the β-**1** film, as measured through a series of flash photolysis experiments, is shifted to higher energy by approximately 900 cm^{-1} from the film absorptance onset (Figure 4, bottom spectrum). For a film containing roughly an equal mixture of the two polymorphs, the triplet formation follows the absorptance onset (Figure 4, top spectrum).

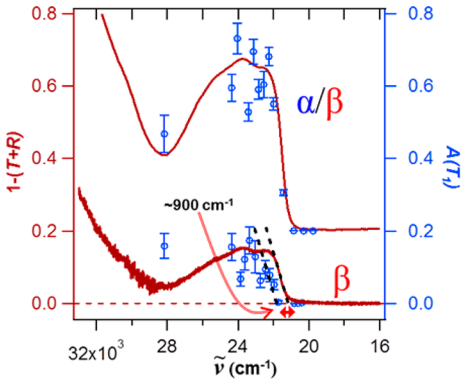

Figure 4. Circles show the triplet action spectra of a mostly β-**1** film (bottom, $\chi_\alpha < 0.1$) and α/β film (top, $\chi_\alpha = 0.45$), monitored at 21 500 cm^{-1} while scanning the excitation energy. The triplet amplitudes are extracted from a monoexponential fit of the decay of the T_1 transient. Solid lines show the absorptance spectra for the corresponding films.

Ultrafast transient absorption measurements as a function of excitation fluence and temperature were carried out to test whether annihilation processes may be affecting triplet formation kinetics and yield. The experiments were carried out on a film of mostly α-**1**, and the concentration profiles were extracted as described above. While there are changes in the excited state kinetics with fluence, the spectral features for the S_1-S_n and T_1-T_n absorptions and the S_0-S_1 bleach are unaffected. The observed decrease in Φ_T at 80 K as a function of increasing fluence (Figure 5) reveals that singlet−singlet annihilation (SSA) plays a role in the excited state kinetic scheme at this temperature.[13] Further evidence for SSA can be found by monitoring the T_1-T_n and S_1-S_n absorption maxima (Figure 5C,D). The kinetic traces in this figure are normalized at short delay times when monitoring S_1-S_n absorption and long delay times when monitoring T_1-T_n absorption, and the traces are fitted with a biexponential function. As the excitation fluence is decreased, there is a clear loss of the fast decay component in S_1 and the corresponding fast rise component in T_1. The fractional amplitude of the fast S_1 decay component ($R_{fast} = A_{fast}/A_{total}$, monitored at 15 000 cm^{-1}) at 80 K is plotted with Φ_T, showing that for the lowest fluences at which Φ_T is highest, the decay of S_1-S_n absorption is described well by a single exponential. The increase in R_{fast} with higher fluence was observed at all temperatures, but the correlation with Φ_T varies. The temperature dependence of Φ_T previously reported[4] is reproduced at low fluences (Figure 5B), but the trend becomes weaker at higher fluences.

Transient spectra on films that are highly enriched in the α polymorph were also recorded at different excitation energies. Figure S6 (SI) compares $[S_1]$ and $[T_1]$ kinetics for a few different fluences at room temperature and shows that the kinetics are similar for those recorded at low and moderate fluences, indicating that a regime where SSA is negligible is accessible. Triplet yields at 30−295 K and representative transient kinetics, acquired at 80 K at different excitation energies across the S_0-S_1 absorption, are presented in Figure 6. Although the error bars for the measurements of Φ_T are quite large (especially at 22 200 cm^{-1} excitation, where the scatter of the excitation beam overlaps strongly with T_1-T_n absorptions), Φ_T generally reaches a maximum of ~2 at 23 810 cm^{-1} excitation (420 nm) at all temperatures, but for 22 200 and 25 800 cm^{-1} excitation Φ_T is reduced at the temperature

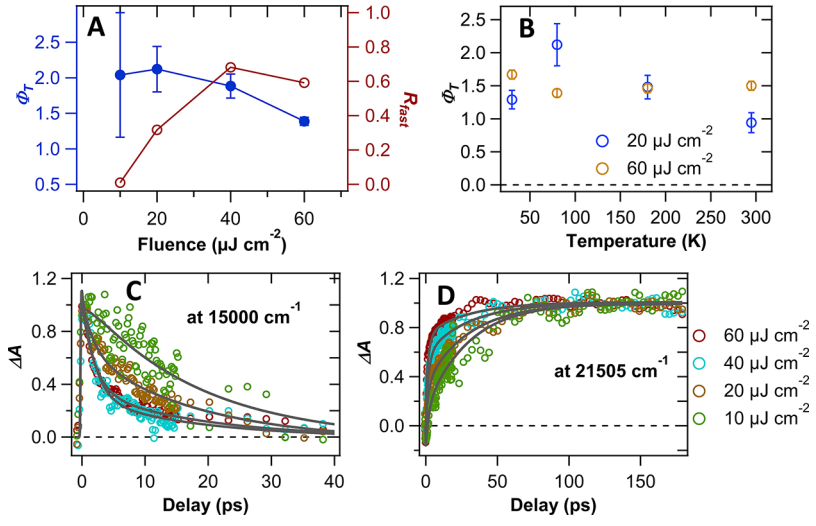

Figure 5. (A) Φ_T and R_{fast} as a function of excitation fluence (25 800 cm^{-1}) at 80 K for an α-rich film ($\chi_\alpha = 0.85$). (B) Temperature dependence of Φ_T at high and low fluences. Normalized kinetics monitoring (C) S_1-S_n (15 000 cm^{-1}) and (D) T_1-T_n (21 505 cm^{-1}) absorption maxima at the indicated fluences at 80 K.

dx.doi.org/10.1021/ja501337b | J. Am. Chem. Soc. 2014, 136, 7363−7373

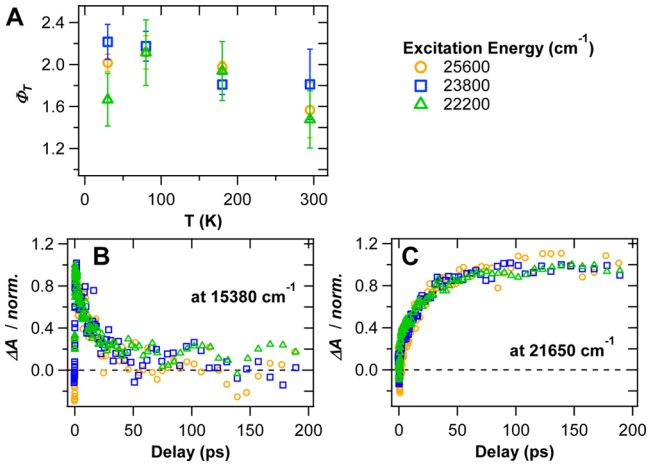

Figure 6. Transient absorption at low fluence (~10 μJ/cm^2) for three different excitation energies. (A) Φ_T of a film composed of mostly α-**1** (χ_α = 0.83), at 30, 80, 180, and 295 K, (B)-(C) Normalized transient dynamics at 80 K as a function of delay time monitoring (B) the decay of the S_1−S_n absorption at 15 380 cm^{-1} and (C) the growth of the T_1−T_n absorption at 21 650 cm^{-1}.

extremes. At high fluences triplet−triplet annihilation (TTA) is observed at delay times greater than 100 ps through monitoring the T_1−T_n absorption maximum, which persists for many nanoseconds with negligible decay at lower fluences.[34] As demonstrated by time-resolved fluorescence data,[8] TTA processes involving free and trapped triplet excitons can occur over time scales extending out to ~50 ns, accounting for the delayed fluorescence. The temperature dependence of these processes, in addition to the likely presence of both polymorphs in any film, accounts for the rich variability observed in the temperature dependent fluorescence spectra (Figure 1).

The possibility of a phase change induced by cooling was explored as a possible additional modifier of Φ_T vs temperature. Cycling the temperature several times from 30 to 295 K before performing a series of transient absorption measurements did not change Φ_T. Allowing the sample to equilibrate at 77 K for only a few minutes vs >1 h prior to measurements also resulted in similar Φ_T. Morphology changes that are fast and reversible may not have been detected using this approach. The absorption spectra of films of α-**1** are very weakly temperature dependent,[4,8] which provides further evidence that a temperature-dependent phase change is unlikely.

Discussion and Modeling. *Excited State Relaxation in Films of β-**1**.* Fitting of the absorption spectra, carried out in the companion paper,[8] reveals that the spectrum of β-**1** can be described by a single Franck−Condon progression, whereas the α-**1** component requires a more complicated H-aggregate model. This suggests that exciton delocalization is more important in the description of α-**1** than in β-**1**, but the similarity to the absorbance of isolated **1** implies that the delocalization is not great in either polymorph. This is in contrast, for example, to the very large differences in the absorption spectra of crystalline versus solution phase linear acenes.[30,35] Excitons in crystalline tetracene, for example, can extend over ~10 molecules, as determined by superradiance.[36]

Fluorescence quantum yields at room temperature increase upon film thermal annealing, from 0.16 for α-**1** to 0.59 for β-**1**, suggesting that excited states of β-**1** decay primarily radiatively. The similarity between the low-temperature fluorescence spectra of α and β films (Figure 1) leads to the conclusion that at low temperatures, when α crystallites are highly efficient at SF, the small amount of β crystallites in these films are dominating the fluorescence. Fluorescence spectra provided in the SI (Figure S1) indicate a broad fluorescent component that underlies the much stronger fluorescence that is presumably from S_1. The broad feature matches closely the excimer emission observed for crystalline perylene films.[8,37] This excimer fluorescence is much more pronounced at higher energy excitations and in β-enriched films. The more strongly fluorescent S_1 state dominates steady-state photoluminescence, and this state can be modeled with a single Franck−Condon progression. The time-resolved fluorescence decays of these films reveal radiative decay from two different states, with lifetimes of 1.3 and 3.3 ns. Similar decay lifetimes are observed, along with two other components, in mostly α-**1** films, again highlighting that even the most highly enriched α-**1** films contain some amount of fluorescent β crystallites.

The triplet action spectra (Figure 4), while containing considerable uncertainty, fit well with a model in which the β-**1** crystallites do not produce two T_1 states from thermalized S_1 but can in higher-lying vibrational levels. XRD studies revealed residual α-**1** features even after extensive annealing;[8] thus, it remains possible that the triplets that are observed in an enriched β-**1** film are arising from a small fraction of α-**1** crystallites present in the sample, which have much higher Φ_T than β-**1** crystallites. However, the onsets in the triplet action and absorptance spectra for mixed films are nearly identical to the absorptance onset for β-**1**, while the triplet onset of β-**1** is blue-shifted, indicating that excess energy above thermalized S_1 is required to produce T_1 in β-**1**. The different triplet onsets for the mixed vs β-**1** films suggest that residual α-**1** is not responsible for the small amount of triplets formed in highly β-**1** films.

The transient spectra at early delay times are dominated by a broad stimulated emission feature that resembles the excimer fluorescence identified in the steady-state fluorescence of β-enriched films (vide supra). The transient spectra of β-**1** films at delay times longer than 100 ps appear somewhat similar to those observed for α-**1** films, and if the transient absorption feature near 21000 cm^{-1} is dominated by T_1−T_n contributions, then comparison of its amplitude with that of the S_0−S_1 bleach feature suggests a much lower Φ_T than in α-**1** films. Since it is known from the high Φ_F that a large number of singlets remain at times longer than 100 ps, S_1−S_S features in this spectral region convoluted with the ground state bleach could also produce transient spectral features that strongly overlap with T_1−T_n and result in the spectrum for β-**1** shown Figure 3C.

The unique triplet action spectrum of β-**1** compared with films enriched in α-**1** (Figure 4) suggests that β-**1** can form triplets only upon excitation with photon energies well in excess of the absorption onset. SSA could also occur at high excitation fluences, promoting **1** to a higher lying S_n state that can undergo SF more readily, which explains the observation under strong excitation of a fast rise component at the position of T_1−T_n absorbance (near 21500 cm^{-1}), even in highly β-**1** films (Figure S3F, SI). A fluence of the appropriate magnitude to incite SSA cannot be achieved in the time-resolved fluorescence experiment; thus, the lack of a fast decay or delayed fluorescence is not evidence against SSA-induced SF. In transient absorption experiments that operate under much higher fluences, the effect is more likely at work, but the triplet yields even at the highest fluences used are still quite low, <0.3.

dx.doi.org/10.1021/ja501337b | J. Am. Chem. Soc. 2014, 136, 7363−7373

Taken together, observations of excited state behavior for β-**1** crystallites strongly imply that the dominant relaxation pathway is fast (<1 ps) formation of a species with excimer character followed by its cooling/trapping and radiative decay. Similar behavior is observed in the two polymorphs of perylene: SF occurs in β-perylene with little excess excitation energy but is suppressed in α-perylene, which forms excimers with rate constants exceeding 10^{12} s^{-1}.[38,39] In β-**1** we label this dominant singlet state as S_1/Ex (Figure 7) and note that as in α-perylene

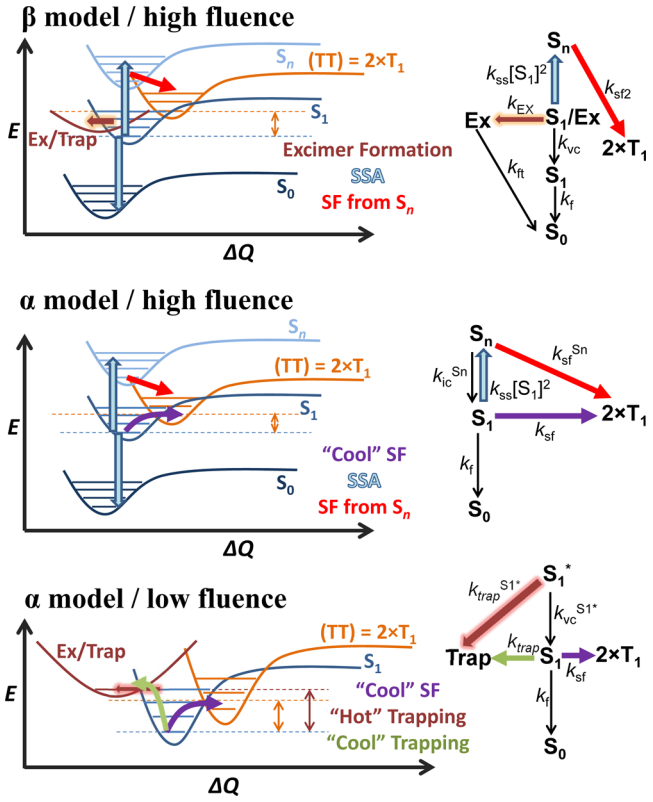

Figure 7. Kinetic schemes for different fluence regimes and film types: (A) β-**1** and high fluence, (B) α-**1** at high fluence, (C) α-**1** at low fluence. Equations for schemes (B) and (C) are in eqs 5 and 6 in SI.

it forms in 1 ps or faster, on the basis of the broad stimulated emission features observed at the earliest times in our ultrafast transient absorption experiment. Evidence is also present for triplet formation via SF that can arise at excitation energies more than 900 cm^{-1} higher than the absorption onset. The mechanism may be due to singlet fission proceeding from higher-lying S_n that is formed via SSA (again, with rise times of less than 2 ps). A separate mechanism may be through a vibrationally hot S_1, similar to SF in α-perylene, where the onset of triplet formation is blue-shifted by 3500 cm^{-1} from that of the β polymorph.[39]

Excited State Relaxation in Films of α-1. The low Φ_F, high Φ_T, and observation of delayed fluorescence are all consistent with SF being the dominant excited state pathway in α-**1** films. The steady-state fluorescence spectra of α-**1** films display a complex temperature dependence (Figure 1). For α-**1** the trend in Φ_T and SF rise times would suggest that fluorescence at 80 K (~200% Φ_T) is nearly entirely delayed in nature, while at higher and lower temperatures other species (e.g., excimers, traps of various types) could be contributing. Also possible is that β-**1**, which was shown to grow near the substrate prior to the growth of α-**1**, is dominating the fluorescence via direct excitation or through energy transfer from α-**1** crystallites. At lower temperatures, fluorescence spectra for a film primarily composed of β-**1** crystallites are very similar to those observed for films enriched in α-**1**. Apparently, the dominant delayed fluorescence signals in α-**1** films at low temperatures arise from similar species as those in β-**1** films, and it is difficult to determine what fraction of the emission arises from the small amount of β-**1** that is present. In the time-resolved fluorescence measurements, the strong presence of decay components associated with β-**1** crystallites is further evidence that the fluorescence of mostly α-**1** films is dominated by the small fraction of β-**1**. Unique fluorescence decay components of α-**1** crystallites are indicative of SF and delayed fluorescence.

The transient absorption spectra of α-**1** films at short delay times match closely the S_1-S_n absorption observed in solutions,[7] and at delay times greater than 100 ps the transient spectra are easily identified as arising from the T_1-T_n absorption, also through comparison with measurements in solution. Transient absorption measurements vs excitation fluence indicate that SSA is an important process that modulates Φ_T and produces the faster triplet rise time. The temperature dependence of the SSA process, or that of a competing process, is evident in the large effect of SSA at low temperatures and the weaker influence at 295 K (Table 1). SSA

Table 1. Extracted Rate Constants from Fits to Transient Data Using α-1/High Fluence Model[a]

T (K)	k_{sf} (ps^{-1})	k_{sf}^{Sn} (ps^{-1})	k_{ss} (cm^{-3} s^{-1})	k_{ic}^{Sn} (ps^{-1})	k_{sf}^{Sn}/k_{ic}^{Sn}
30	0.023	5.0	8.7×10^{-9}	1.1	4.5
80	0.028	6.0	8.9×10^{-9}	1.0	6.0
180	0.025	5.0	5.0×10^{-9}	1.9	2.6
295	0.030	5.0	5.2×10^{-9}	1.6	3.1

[a] k_f held at 0.0003 ps^{-1} in these fits.

still results in the formation of T_1, but if it were the only mechanism of triplet formation the maximum Φ_T would be 100% because half of the S_1 excitons are lost in the SSA process. Thus, in systems where SF is fast and barrierless from S_1, SSA is a loss mechanism and is avoided by extrapolation to very low fluence conditions. However, in mixed films of **1** some gain in Φ_T could result at higher fluences because the SF rate constant increases sharply with excess energy given to the singlet species of β-**1** that, when fully relaxed, is unlikely to undergo SF. The unique temperature dependence of Φ_T at high versus low fluence is evidence that the impact of SSA on the dynamics is temperature dependent.

TTA is revealed by the delayed fluorescence observed for α-**1** films; the low fluence conditions of the time-resolved fluorescence experiment result in a lifetime for the delay fluorescence of ~17 ns. At the higher fluences used in the transient absorption experiment, higher overall concentrations of T_1 are produced and the delayed fluorescence lifetime is likely shorter.

Under low fluence conditions, at 25 800 cm^{-1} excitation and temperatures other than 80 K, Φ_T is lower than the maximum of 2, indicating that a loss mechanism other than SSA is operative. This process may be trapping or excimer formation from S_1 or internal conversion from S_1 that competes with the ~25 ps SF process. Φ_T values recorded at 30, 80, 180, and 295 K after low fluence excitation at different energies across the S_0-S_1 absorption (Figure 6) indicate that the excitation energy

dx.doi.org/10.1021/ja501337b | J. Am. Chem. Soc. 2014, 136, 7363−7373

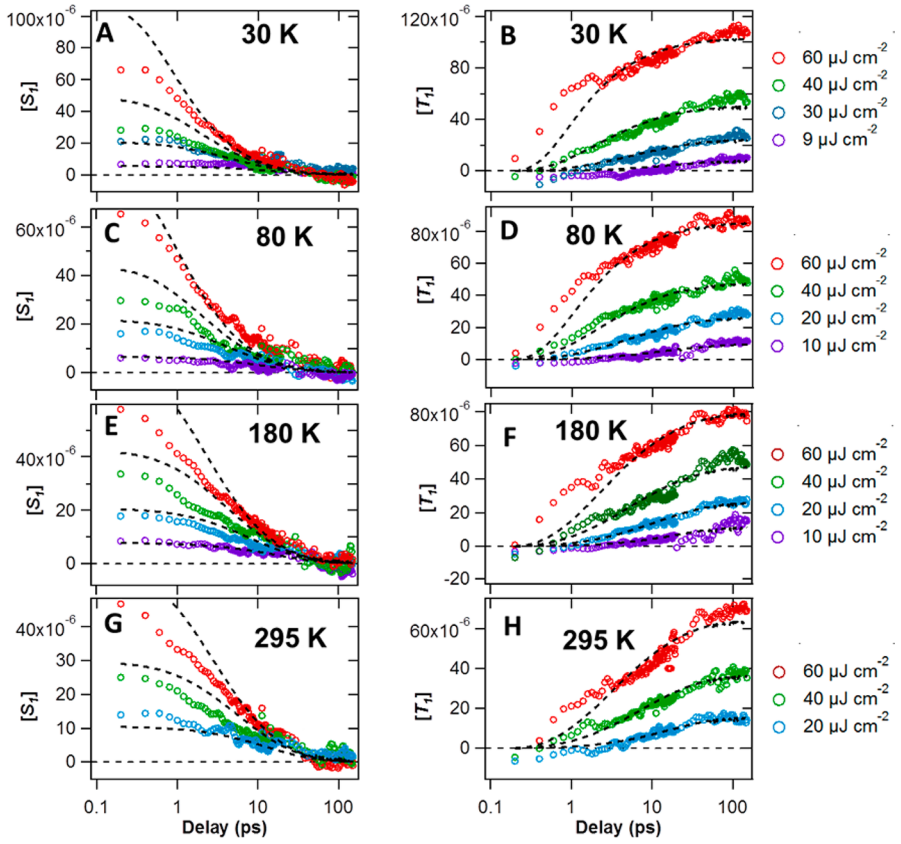

Figure 8. Fits with the α-**1**/high fluence model. Global fits (dashed lines) of (A) $[S_1]$ and (B) $[T_1]$ (both in mol cm^{-3}) of a highly α film ($\chi_\alpha = 0.85$) across a range of fluences: (A, B) 30 K (the fluences are indicated in the legend to the right of panel B), (C, D) 80 K, (E, F) 180 K, and (G, H) 295 K. The best fit parameters are presented in Table 1

is also an important factor in the fate of the initially prepared S_1 species. The Φ_T values and $[S_1]$ and $[T_1]$ kinetics recorded after excitation at various energies at low fluences do not show a monotonic trend that is associated, for example, with faster triplet formation when SF is more exothermic; rather, at 30 and 295 K Φ_T reaches a maximum at 23 810 cm^{-1} excitation, near the peak of the S_0-S_1 absorption, and decreases at higher and lower excitation energies. At 80 and 180 K, the Φ_T values at the different excitation energies are within error of each other, and near the maximum of 2. The $[T_1]$ and $[S_1]$ kinetics (presented in Figure 9) recorded at low fluence do not contain the rapid components observed at higher fluences and attributed to SSA. The high Φ_T at 23 810 cm^{-1} excitation may indicate that there is a SF contribution arising from a vibrationally excited level of S_1. This is the case, for example, in the SF dynamics of rubrene, which shows two time constants for SF of 2 and 25 ps;[40,41] the faster time constant for SF has been attributed to "direct" SF from a vibrationally hot state, while the slower time constant arises from a thermally activated fission process.[40] k_{sf} also changes dramatically across the linear acene series (anthracene, tetracene, pentacene) as the $S_1-2\times T_1$ splitting increases.[1] The lack of a rapid T_1 formation component at higher excitation energies observed in Figure 9 indicates that if SF is occurring from higher-lying vibrational levels of S_1, it is not nearly as rapid as in rubrene. The decrease in Φ_T at excitation energies higher than 23 810 cm^{-1} may be indicative of strongly activated excimer or trap formation. The lower Φ_T at 22 200 cm^{-1}, close to the S_0-S_1 absorption onset, arises from a competition between SF and trapping, both of which have barriers from the bottom of S_1.

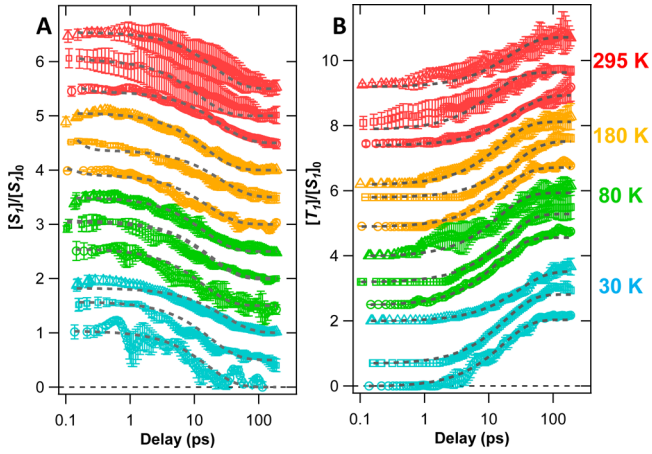

Figure 9. Fits with the low fluence α-**1** model. Global fits of (A) $[S_1]$ and (B) $[T_1]$ at 30, 80, 180, and 295 K at three different excitation energies. The data and fits are normalized by the initial $[S_1]$ and offset for clarity. Circles, excitation at 25 600 cm^{-1}; squares, excitation at 23 800 cm^{-1}; triangles, excitation at 22 200 cm^{-1}. The films have a high α-**1** content, with $\chi_\alpha = 0.85$. The error bars are one standard deviation of the extracted concentration, from measurements that sample several locations on the film.

On the basis of the observations described above we aim to develop a model that is capable of fitting $[S_1]$ and $[T_1]$ concentration profiles vs time delay t at different fluences and correctly reproduces the temperature dependence of Φ_T. A simple model is used (Figure 7, middle) to first assess the role of SSA as a function of fluence. The α-**1**/high fluence model

dx.doi.org/10.1021/ja501337b | J. Am. Chem. Soc. 2014, 136, 7363−7373

Table 2. Extracted Rate Constants from the Global Fitting of the Fluence-Dependent Data Sets Using the α-1/Low-Fluence Model (all rate constants are ps^{-1})[a]

T (K)	excitation (cm^{-1})	Φ_T	k_{sf}	k_{sf} (avg)	k_{vc}	k_{trap}^{S1*}	k_{trap}
30	2.22×10^4	1.67 ± 0.25	0.031		13.6	0.0001	0.0021
	2.38×10^4	2.22 ± 0.17	0.055	0.049 ± 0.015	16.0	0.0001	0.0001
	2.56×10^4	2.02 ± 0.16	0.060		12.9	0.0770	0.0001
80	2.22×10^4	2.11 ± 0.31	0.066		15.2	0.0001	0.0011
	2.38×10^4	2.17 ± 0.14	0.055	0.064 ± 0.008	15.8	0.0001	0.0001
	2.56×10^4	2.11 ± 0.16	0.071		16.0	0.0150	0.0001
180	2.22×10^4	1.94 ± 0.28	0.060		16.1	0.0001	0.0050
	2.38×10^4	1.81 ± 0.10	0.038	0.052 ± 0.013	14.9	0.6000	0.0001
	2.56×10^4	1.98 ± 0.05	0.060		14.1	1.8900	0.0001
295	2.22×10^4	1.48 ± 0.27	0.035		16.1	0.0154	0.0124
	2.38×10^4	1.81 ± 0.34	0.073	0.047 ± 0.023	15.4	0.5900	0.0127
	2.56×10^4	1.57 ± 0.26	0.032		15.0	1.1100	0.0071

[a] k_f held at 0.0003 ps^{-1} in these fits.

includes SSA, fast SF from the S_n prepared via SSA that competes with internal conversion back to S_1, and a slower SF process that occurs directly from S_1 to $2 \times T_1$, accounting for the entire triplet population at sufficiently low fluences. TTA is not included in the α-1/high fluence model, which aims only to describe the kinetics at delay times shorter than 1 ns. Fast triplet formation via SSA to S_n accounts for the initial rapid rise in $[T_1]$ over the first few picoseconds. S_n sits well above the threshold for SF, and the model assumes that SF is extremely efficient once S_n is formed. This is the case, for example, in rubrene crystals that have SF time constants of 2 and 20 ps when excited near the absorption onset but display much faster SF ($\tau \sim 200$ fs) when excited into higher S_n.[41] In addition to the higher exothermicity of SF from S_n increasing the rate constant for SF, accessing higher S_n may also promote SF through accessing intermolecular vibrations that prepare intermolecular geometries poised to generate ^{1}(TT).[20] Figure 8 shows a global fit of fluence-dependent measurements at 30, 80, 180, and 295 K. The fits were carried out through numerical integration of the series of differential equations that describe the α-1/high fluence model (eq S5, SI). All of the rate constants were treated as global variables, and the initial $[S_1]$ concentration was linked between the solutions of $[S_1](t)$ and $[T_1](t)$ at a given fluence. The best fit parameters are presented in Table 1.

The equations resulting from the α-1/high fluence model provide satisfactory fits to the data. The best fits of the fluence-dependent data sets reveal that the rate constant for SSA, k_{ss}, decreases as temperature is increased, from $\sim 9 \times 10^{-9}$ cm^{-3} s^{-1} at 30 K to $\sim 5 \times 10^{-9}$ cm^{-3} s^{-1} at room temperature. These values are comparable to the SSA rate constant recently reported for amorphous films of 5,12-diphenyltetracene ($k_{ss} = 3.9 \times 10^{-9}$ cm^{-3} s^{-1})[13] and slightly lower than that of tetracene films ($k_{ss} = 1.7 \times 10^{-8}$ cm^{-3} s^{-1}).[42] SSA is more pronounced at lower temperatures, perhaps indicating longer diffusion lengths at these temperatures[43] or reflecting the contraction of the unit cell as the crystal is cooled.[8] k_{sf} roughly follows the observed temperature dependence of Φ_T. The ratio k_{sf}^{Sn}/k_{ic}^{Sn} indicates that SF is highly efficient from S_n, and k_{sf}^{Sn} values imply a time constant for this process of ~200 fs. The fluorescence rate constant k_f is small enough to have negligible effect on the fit over the time window of the experiment and was held near the value observed in time-resolved fluorescence experiments.

A shortcoming of the α-1/high fluence model is the poor fit of $[S_1]$ over the first few hundred femtoseconds for data sets recorded at the highest fluences. Constraining the fitted $[S_1]$ to be equal to the observed initial value resulted in poor fits to both the $[S_1](t)$ and $[T_1](t)$ profiles in all cases. We attribute the poor fits at the highest fluences to rapid S_1 decays within the instrument response as a result of SSA. This is consistent with the slight increase in Φ_T that is observed at higher fluences (e.g., Figure 5B), because the observed initial $[S_1]$ is defined after 400 fs of population evolution, and if it is already slightly depopulated, Φ_T becomes inflated. We note that the overshoot of $[S_1]$ in fits of α-1 films mentioned above may also be due to altered peak molar extinction coefficients compared with solution or incomplete separation of S_1-S_n and T_1-T_n spectra due to their considerable overlap and convolution with the instrument response at short delay times. Allowing the peak extinction coefficients to vary such that the fit improves also modifies the calculated Φ_T, but by a factor smaller than our reported uncertainty. The α-1/high fluence model also tends to underestimate $[S_1]$ at longer delay times for high excitation fluences, which could result from not accounting for TTA processes that feed population back to S_1.

Next we examine the kinetics at low fluence in the absence of SSA using a model (Figure 7, bottom) that accounts for excitation energy dependent Φ_T values. A trap state, such as the excimer that dominates the excited state dynamics in β-1 films, is invoked as a competitor to SF to account for $\Phi_T < 2$. The excitation energy dependent Φ_T values are rationalized by introducing a trapping process from the initially prepared (hot) S_1 state (S_1*) that competes with vibrational cooling on the S_1 surface, as well as an additional slower trapping process from the thermalized S_1. The coupled differential equations describing this model are presented in eq 6 of the SI. The data and fits using these equations are presented in Figure 9, and the best fit parameters can be found in Table 2.

The best fit parameters reveal that "hot" trapping is an important contributor to α-1 photophysics at higher excitation energies: k_{trap}^{S1*} increases with increasing excitation energy, and this trend is the most pronounced at 180 and 295 K. At most temperatures and excitation energies Φ_T is very close to 2, and in these cases trapping is minimal. The fits also indicate a weaker impact from trapping via thermalized excitations as temperature decreased below 295 K, consistent with an activation barrier to trapping from the bottom of S_1. k_{sf} varies for different excitation energies at a given temperature, but the values remain within the considerable uncertainty for the low-fluence measurements. k_{sf} does not track the excitation energy

dx.doi.org/10.1021/ja501337b | J. Am. Chem. Soc. 2014, 136, 7363−7373

or change significantly with temperature, so there does not seem to be any evidence for SF from vibrationally excited levels or for a significant barrier to SF. Although the calculated energetic barrier is approximately 800 cm^{-1}, entropic contributions could facilitate SF, as has been discussed for tetracene.[27]

In summary, the analysis of the low-fluence variable temperature and excitation energy kinetics of $[S_1]$ and $[T_1]$ supports a nearly temperature independent rate of SF, but trapping becomes a significant competitor of SF at higher excitation energies and at temperatures above 180 K.

Connection between Polymorph Structure and Photophysics. Current theories emphasize the role that π-stacking—particularly slip-stacking—of chromophores plays in optimizing the matrix element for SF.[1,5] As discussed at length in the companion paper,[8] the crystalline packing in both polymorphs leads to very similar π-stacking interactions that form slip-stacked columns. Differences exist in the longer-range order of the crystals; for example, while the unit cells of both α-**1** and β-**1** contain four translationally inequivalent molecules, the unit cell volume of β-**1** is smaller than that of α-**1**. In addition, the interaction geometries between slip-stacked columns are different in the two polymorphs.

The different fates of S_1 despite the very similar "dimer" geometries is something that cannot be explained using existing theories of the role of interchromophore coupling in SF. Rather, the differences in longer range packing may promote the fast formation of a stable excimer-like species in β-**1**, relative to that in α-**1**. Modeling the transient dynamics of α-**1** films (Figure 9) showed that rapid trap/excimer formation from higher-lying vibrational levels of S_1 can be an important modifier of Φ_T, and at significantly high temperatures, trap/excimer formation can also occur from the thermalized S_1. At high energy excitation, trap/excimer formation occurs with $k_{trap}^{S1*} = 1-2\ ps^{-1}$, but it is competing with vibrational cooling on the S_1 surface that is much faster, $k_{vc} = 13-16\ ps^{-1}$. If the same k_{vc} rate constants are assumed for β-**1**, formation of the species responsible for the strong stimulated emission feature observed at $t < 200$ fs in our transient absorption experiment requires a rate constant comparable to k_{vc} and leaves k_{EX} (the main competition with k_{sf} in β-**1**) about an order of magnitude larger than k_{trap}^{S1*} (the main competition with k_{sf} in α-**1**).

The longer-range crystalline structure appears to also influence the energy of S_1, as indicated by a 600 cm^{-1} blue shift in the onset of absorption for α-**1** compared to β-**1**. The lower S_1 energy in β-**1** should mean that SF is significantly more endergonic than in α-**1**, which is evident in the transient studies presented here.

IV. CONCLUSIONS

The concentrations $[T_1]$ and $[S_1]$ as a function of time were extracted from the ultrafast transient absorption data sets for α-**1** films and were modeled to better understand the SF mechanism in these films. Studies of the fluence dependence of excited state kinetics indicate that the two time scales for triplet formation in α-**1** films arise from (1) singlet−singlet annihilation processes to form a S_n state that fissions extremely quickly and (2) a slower fission pathway involving SF from S_1 to $2 \times T_1$. A study of the transient kinetics carried out at low fluences, in the absence of SSA, has provided insight into the role of trapping processes in attenuating Φ_T. A "hot" trapping process is active for excitations well above the absorption onset, while trapping from the thermalized S_1 is important at temperatures above 180 K, consistent with an activation barrier for this process. k_{sf} rate constants are essentially temperature-independent.

UV−vis absorption and triplet action spectra indicate that SF is significantly slower than competing processes from the thermalized S_1 level of β-**1** crystallites, but a small triplet yield is attained at higher energy excitations. Time-resolved spectroscopy and fluorescence measurements show that the singlet state quickly formed in β-**1** possesses excimer character and decays mostly radiatively. The diverse behavior observed in films composed of just one type of SF molecule underscores the defining role that even longer-range molecular ordering plays in determining the efficiency of SF.

■ ASSOCIATED CONTENT

Ⓢ Supporting Information

Fluorescence excitation spectra (Figure S1), transient absorption on drop-cast films (Figure S2), full transient absorption data sets for annealed films (Figure S3), details of quantum yield determination including molecular orientation factors (Figures S4 and S5, Table S1), transient absorption data vs temperature and excitation fluence (Figures S6-S8), and a full description of the models used in global fitting (equations S5 and S6). This material is available free of charge via the Internet at http://pubs.acs.org.

■ AUTHOR INFORMATION

Corresponding Author

Justin.Johnson@nrel.gov

Notes

The authors declare no competing financial interest.

■ ACKNOWLEDGMENTS

This work has been supported by the U.S. Department of Energy, Office of Basic Energy Sciences, Division of Chemical Sciences, Biosciences, and Geosciences. J.N.S., J.R., and J.C.J acknowledge contract no. DE-AC36-08GO28308 with NREL, and J.M. acknowledges Award Number DOE DE-SC0007004.

■ REFERENCES

(1) Smith, M.; Michl, J. *Chem. Rev.* **2010**, *110*, 6891 and references therein..

(2) Hanna, M. C.; Nozik, A. J. *J. Appl. Phys.* **2006**, *100*, 074510.

(3) Johnson, J. C.; Akdag, A.; Zamadar, M.; Chen, X. D.; Schwerin, A. F.; Paci, I.; Smith, M. B.; Havlas, Z.; Miller, J. R.; Ratner, M. A.; Nozik, A. J.; Michl, J. *J. Phys. Chem. B* **2013**, *117*, 4680.

(4) Johnson, J. C.; Nozik, A. J.; Michl, J. *J. Am. Chem. Soc.* **2010**, *132*, 16302.

(5) Johnson, J. C.; Nozik, A. J.; Michl, J. *Acc. Chem. Res.* **2013**, *46*, 1290.

(6) Paci, I.; Johnson, J. C.; Chen, X.; Rana, G.; Popović, D.; David, D. E.; Nozik, A. J.; Ratner, M. A.; Michl, J. *J. Am. Chem. Soc.* **2006**, *128*, 16546.

(7) Schwerin, A. F.; Johnson, J. C.; Smith, M. B.; Sreearunothai, P.; Popovic, D.; Cerny, J.; Havlas, Z.; Paci, I.; Akdag, A.; MacLeod, M. K.; Chen, X. D.; David, D. E.; Ratner, M. A.; Miller, J. R.; Nozik, A. J.; Michl, J. *J. Phys. Chem. A* **2010**, *114*, 1457.

(8) Ryerson, J.; Schrauben, J.; Ferguson, A.; Sahoo, S.; Naumov, P.; Havlas, Z.; Michl, J.; Nozik, A. J.; Johnson, J. C. 2014, Submitted to *J. Phys. Chem. C.*

(9) Dillon, R. J.; Piland, G. B.; Bardeen, C. J. *J. Am. Chem. Soc.* **2013**, *135*, 17278.

(10) Ramanan, C.; Smeigh, A. L.; Anthony, J. E.; Marks, T. J.; Wasielewski, M. R. *J. Am. Chem. Soc.* **2012**, *134*, 386.

(11) Eaton, S. W.; Shoer, L. E.; Karlen, S. D.; Dyar, S. M.; Margulies, E. A.; Veldkamp, B. S.; Ramanan, C.; Hartzler, D. A.; Savikhin, S.; Marks, T. J.; Wasielewski, M. R. *J. Am. Chem. Soc.* **2013**, *135*, 14701.
(12) Chan, W. L.; Berkelbach, T. C.; Provorse, M. R.; Monahan, N. R.; Tritsch, J. R.; Hybertsen, M. S.; Reichman, D. R.; Gao, J. L.; Zhu, X. Y. *Acc. Chem. Res.* **2013**, *46*, 1321.
(13) Roberts, S. T.; McAnally, R. E.; Mastron, J. N.; Webber, D. H.; Whited, M. T.; Brutchey, R. L.; Thompson, M. E.; Bradforth, S. E. *J. Am. Chem. Soc.* **2012**, *134*, 6388.
(14) Wilson, M. W. B.; Rao, A.; Clark, J.; Kumar, R. S. S.; Brida, D.; Cerullo, G.; Friend, R. H. *J. Am. Chem. Soc.* **2011**, *133*, 11830.
(15) Wang, C.; Tauber, M. J. *J. Am. Chem. Soc.* **2010**, *132*, 13988.
(16) Kuhlman, T. S.; Kongsted, J.; Mikkelsen, K. V.; Moller, K. B.; Solling, T. I. *J. Am. Chem. Soc.* **2010**, *132*, 3431.
(17) Johnson, J. C.; Reilly, T. H.; Kanarr, A. C.; van de Lagemaat, J. *J. Phys. Chem. C* **2009**, *113*, 6871.
(18) Marciniak, H.; Pugliesi, I.; Nickel, B.; Lochbrunner, S. *Phys. Rev. B* **2009**, *79*, 235318.
(19) Zimmerman, P. M.; Bell, F.; Casanova, D.; Head-Gordon, M. *J. Am. Chem. Soc.* **2011**, *133*, 19944.
(20) Grumstrup, E. M.; Johnson, J. C.; Damrauer, N. H. *Phys. Rev. Lett.* **2010**, *105*, 257403.
(21) Moller, W. M.; Pope, M. *J. Chem. Phys.* **1973**, *59*, 2760.
(22) Renaud, N.; Sherratt, P. A.; Ratner, M. A. *J. Phys. Chem. Lett.* **2013**, *4*, 1065.
(23) Smith, M. B.; Michl, J. *Annu. Rev. Phys. Chem.* **2013**, *64*, 361.
(24) Greyson, E. C.; Stepp, B. R.; Chen, X. D.; Schwerin, A. F.; Paci, I.; Smith, M. B.; Akdag, A.; Johnson, J. C.; Nozik, A. J.; Michl, J.; Ratner, M. A. *J. Phys. Chem. B* **2010**, *114*, 14223.
(25) Greyson, E. C.; Vura-Weis, J.; Michl, J.; Ratner, M. A. *J. Phys. Chem. B* **2010**, *114*, 14168.
(26) Johnson, R. C.; Merrifield, R. E. *Phys. Rev. B* **1970**, *1*, 896.
(27) Wilson, M. W. B.; Rao, A.; Johnson, K.; Gélinas, S.; di Pietro, R.; Clark, J.; Friend, R. H. *J. Am. Chem. Soc.* **2013**, *135*, 16680.
(28) Burdett, J. J.; Gosztola, D.; Bardeen, C. J. *J. Chem. Phys.* **2011**, *135*, 214508.
(29) Burdett, J. J.; Muller, A. M.; Gosztola, D.; Bardeen, C. J. *J. Chem. Phys.* **2010**, *133*, 144506.
(30) Spano, F. C. *Acc. Chem. Res.* **2010**, *43*, 429.
(31) The estimate is based on a highly α film of 190 nm thickness with an absorbance of ∼2.5 at 24 000 cm^{-1}, reported in ref 8. The reported density of 1.29 g cm^{-3} was used to calculate the concentration of **1** in its crystalline form.
(32) These concentrations are extracted by fitting the spectrum at a given pump−probe delay with the expression $d([S_1]\varepsilon_{S1} + [T_1]\varepsilon_{T1} - [S_0]\varepsilon_{S0})$, where d is the film thickness, taken as 100 nm for all of the fitting done in this report.
(33) The error in $[T_1]$ reflects the variability in the extracted $[T_1]$ in the time window of 160−170 ps, well after T_1 is fully formed. This variability in $[T_1]$ arises from instrumental noise, primarily due to instability in the pump and probe power. A similar error is not presented for $[S_1]$ because this state depopulates rapidly.
(34) For these films it can be difficult to assign a definitive rate constant for triplet fusion because the films undergo photodamage at higher fluences, which can manifest as a decay in the T_1-T_n signal that resembles triplet fusion.
(35) Spano, F. C. *Annu. Rev. Phys. Chem.* **2006**, *57*, 217.
(36) Lim, S. H.; Bjorklund, T. G.; Spano, F. C.; Bardeen, C. J. *Phys. Rev. Lett.* **2004**, *92*, 107402.
(37) Seko, T.; Ogura, K.; Kawakami, Y.; Sugino, H.; Toyotama, H.; Tanaka, J. *Chem. Phys. Lett.* **1998**, *291*, 438.
(38) Albrecht, W. G.; Michelbeyerle, M. E.; Yakhot, V. *Chem. Phys.* **1978**, *35*, 193.
(39) Albrecht, W. G.; Michel-Beyerle, M. E.; Yakhot, V. *J. Lumin.* **1979**, *20*, 147.
(40) Ma, L.; Zhang, K.; Kloc, C.; Sun, H.; Soci, C.; Michel-Beyerle, M. E.; Gurzadyan, G. G. *Phys. Rev. B* **2013**, *87*, 201203.
(41) Ma, L.; Zhang, K. K.; Kloc, C.; Sun, H. D.; Michel-Beyerle, M. E.; Gurzadyan, G. G. *Phys. Chem. Chem. Phys.* **2012**, *14*, 8307.
(42) Tayebjee, M. J. Y.; Clady, R. G. C. R.; Schmidt, T. W. *Phys. Chem. Chem. Phys.* **2013**, *15*, 14797.
(43) The diffusion length in tetracene crystals increases exponentially as the temperature is lowered (Vaubel, G.; Baessler, H. *Mol. Cryst. Liq. Cryst.* **1970**, *12*, 47). In contrast, exciton diffusion in conjugated polymers (Mikhnenko, O. V.; Cordella, F. *J. Phys. Chem. B* **2008**, *112*, 11601) is temperature-independent at low temperatures (4−150 K) and temperature-dependent at higher temperatures, arising from activated hopping.